JMEPEG (2009) 18:959–965
DOI: 10.1007/s11665-008-9309-2

1059-9495/$19.00

Studies on Hot Corrosion of the Microstructurally Different Regions of 2.25Cr-1Mo (T22) Boiler Tube Steel Weldment

Ravindra Kumar, V. K. Tewari, and Satya Prakash

(Submitted December 5, 2007; in revised form August 27, 2008)

This study examines the effect of microstructurally different regions on the hot corrosion of tungsten inert gas weldment in 2.25Cr-1Mo (T22) boiler tube steel. Various regions of weldment were oxidized in molten salt Na_2SO_4-60% V_2O_5 environment at 900 °C. The base metal was found to oxidize at much higher rates than the weld metal and the heat-affected zone. Oxide scales formed in the three regions were compared by scanning electron microscopy with energy dispersive of X-ray analysis, X-ray diffraction pattern, and electron probe microanalysis. The research investigates the formation of inner scales with free Cr over the HAZ.

Keywords boiler tube steel, hot corrosion, molten salt, tungsten inert gas (TIG), weldment

1. Introduction

Chromium-molybdenum steels are extensively used in the steam generator circuits of power plants. These components may require welding of the cracks that can develop during fabrication, storage, and transportation stages, or during the service life of the plant. The microstructures of Cr-Mo steels are very susceptible to thermo mechanical treatments. This microstructural susceptibility is often exploited to develop carbide precipitates of a required chemistry, morphology, and distribution to affect precipitation hardening (Ref 1, 2). Welding is by far the most important of the processes to which structural alloy steels are subjected during the different stages of fabrication. When the ferritic steels are fusion welded, sharp changes are caused in the microstructure of the weldment depending upon the welding parameters. Metallurgical transformations that occur during welding result from thermal cycles and wide range of cooling rates experienced by the different regions of the weldments. A strong need, therefore, exists for the simulation of the conditions under which different microstructures could be produced so as to understand the spectrum of microstructures encountered in the specimen, starting from the weld metal through the heat-affected zone (HAZ). Hot corrosion is the accelerated oxidation of materials at elevated temperatures induced by a thin film of fused salt deposit (Ref 3). The failure of boiler tubes due to fireside corrosion in a waste heat recovery boiler utilizing the exhaust of a gas turbine fired with high speed diesel has been analysed by Srikanth et al. (Ref 4). They reported that the corrosion occurs because of the reaction of the sulfur species in the gas phase with metal surfaces. The sulfur present in coal and fuel oils yields SO_2 on combustion which is partially oxidized to SO_3. The NaCl (either as impurities in the fuel or in the air) reacts with SO_3 and water vapor at combustion temperature to yield Na_2SO_4. Small amount of vanadium may also be present in fuel oils which on combustion forms V_2O_5. This may further react with Na_2SO_4 to form low melting sodium vanadate, which are extremely corrosive to high temperature materials used in the combustion system as discussed by Khanna and Jha (Ref 5) and Hwang and Rapp (Ref 6).

The present study has been carried out to asses the hot corrosion behavior of base metal, weld metal, and HAZ regions of TIG weldment in 2.25Cr-1Mo boiler tube steel in Na_2SO_4-60% V_2O_5 at 900 °C. A SEM back scattered image analysis of the cross section of the oxide scale thickness has been made to measure the oxide scales formed over the regions namely weld metal, HAZ, and base metal. Oxide scale formed over the different regions of TIG weldment have been characterized using X-ray diffraction (XRD), electron probe microanalysis (EPMA), and scanning electron microscopy/energy-dispersive analysis (SEM/EDAX).

2. Experimental Procedure

2.1 Materials and Preparation of Weld

SA 213 2.25Cr-1Mo (T22) boiler tube steel was procured from thermal power plant Bhatinda (India). This steel tube (10 mm thickness × 25 mm diameter) was machined for making V-groove with bevel angle 30°, root face of 1 mm and root gap 1 mm. Tubes were welded together by tungsten inert gas (TIG) welding using 99% pure argon gas as shielded gas with filler wire AWS A 5.28 ER90S-B3. The nominal chemical

Ravindra Kumar, V. K. Tewari, and **Satya Prakash**, Metallurgical and Materials Engineering Department, Indian Institute of Technology Roorkee, Roorkee 247667, India. Contact e-mail: ravirs_2002@rediffmail.com.

compositions of the base metal and the deposited filler wire are given in Table 1. The welding parameters were published in an earlier paper by Kumar et al. (Ref 7).

2.2 Metallography and Specimen Preparation

The cross section of the weldment portion was polished, etched with 2% nital for 20 s and then examined by optical microscopy. Microsturucturally different regions, i.e., base metal, weld metal, and HAZ were identified. The structures of these regions are shown in Fig. 1. Using a diamond precision wafering blade specimens of weld metal, HAZ and base metal were cut out from the weldment in the approximate size $15 \times 5 \times 2$ mm^3 and polished with 220 grades of SiC paper and emery paper and then wheel polished before corrosion test.

2.3 Hot Corrosion Test

The cyclic oxidation studies for weld metal, HAZ and base metal regions of TIG weldment were conducted in Na_2SO_4-60% V_2O_5 at 900 °C for 50 cycles. Each cycle consisted of 1 h heating at a given temperature in a silicon carbide tube furnace followed by 20 min cooling at ambient conditions. The specimens were kept in alumina boats and then the boats were inserted in the furnace. The aim of cyclic hot corrosion is to create accelerated conditions for testing. The specimens were wheel cloth polishing before corrosion test. The coating of uniform thickness with 3-5 mg/cm^2 of Na_2SO_4-60% V_2O_5 was applied with a camel hair brush on the preheated sample (250 °C). The samples were examined at the end of each cycle and subjected to weight change measurements. The electronic balance machine Model 06120 (Contech, India) with a sensitivity of 1 mg was used to measure the weight change values. The spalled scale was also included at the time of measurements of weight change to determine total rate of oxidation. The samples after oxidation were analyzed by SEM/EDAX and XRD for surface analysis. The samples were then cut and mounted for the cross-sectional oxide scale thickness measurement and EPMA.

Table 1 Chemical composition (wt.%) for 2.25Cr-1 Mo boiler tube steel and filler wire used in the present study

	Chemical composition, wt.%							
Materials	**C**	**Mn**	**Si**	**S**	**P**	**Cr**	**Mo**	**Fe**
Base metal	0.15	0.3-0.6	0.5	0.03	0.03	1.9-2.6	0.87	Balance
Filler wire	0.10	0.62	0.48	0.006	0.009	2.55	1.08	Balance

3. Results and Discussion

3.1 Microstructure

The microstructures of the base metal, weld metal, and HAZ regions of the weldment are different. The weld metal shows a combination of widmanstatten type ferrite, pearlite, and bainite. The presence of Cr and Mo in the alloy enhances hardenability and promotes bainite formation even on relatively slow cooling

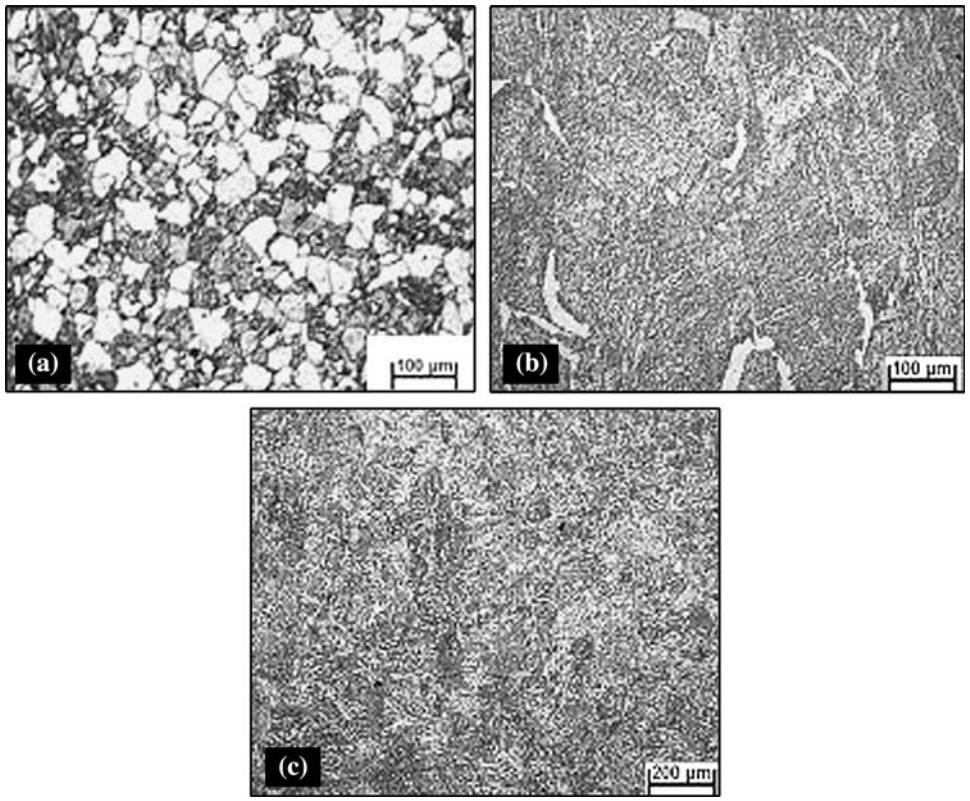

Fig. 1 Optical micrographs of the etched microstructures in the different region of the weldment of 2.25Cr-1Mo steel (a) base metal, 250×, (b) weld metal, 100×, and (c) coarse grain bainite in HAZ, 100×

(Fig. 1b) as also suggested by Natarajan and Babu (Ref 8). The HAZ region showed coarse grain bainite (Fig. 1c). The microstructures of base metal show ferrite (white constituent) and pearlite (dark constituent); those could be resolved at certain locations showing alternate lamellas of ferrite and cementite (Fig. 1a).

3.2 Cyclic Oxidation in Molten Salt

Cumulative weight change (mg/cm^2) variation as a function of time expressed in number of cycles for different regions of TIG weldment is shown in Fig. 2. Intense spalling was observed through out the experimentation on base metal. As soon as subscale forms the top layer of scale breaks away from it and the separated multiple layers overlapping each other were seen. It was observed that for weld metal, the color of the surface scale turned black during the first cycle. Spalling of oxide scale was observed during the third cycle. Even little cracks appeared on the scale at 13th cycles, after that there was increase in the number and width of these cracks and protrusion of oxides from these cracks was observed. The color of the scale was dark gray after the 50th cycle. In case of HAZ black gray color was observed on this region during first cycle. A thin layer of oxide scale got spalled during 17th cycle. The scale of HAZ specimen started cracking during 32nd cycle. The scale was protruded out at the edges in subsequent cycles. In base metal intense spalling and cracking was observed up to 50th cycle.

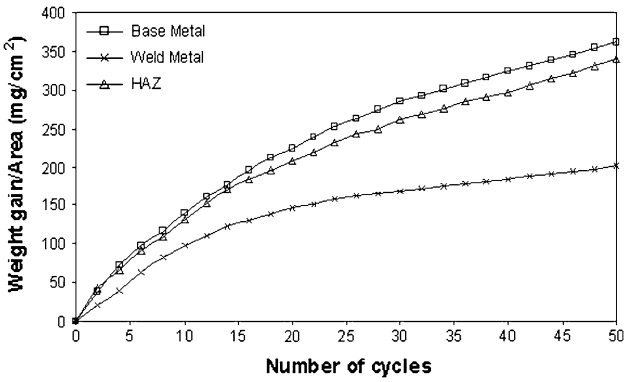

Fig. 2 Weight gain plot for different regions of TIG weldment in T22 steels exposed to Na_2SO_4-60% V_2O_5 at 900 °C for 50 cycles

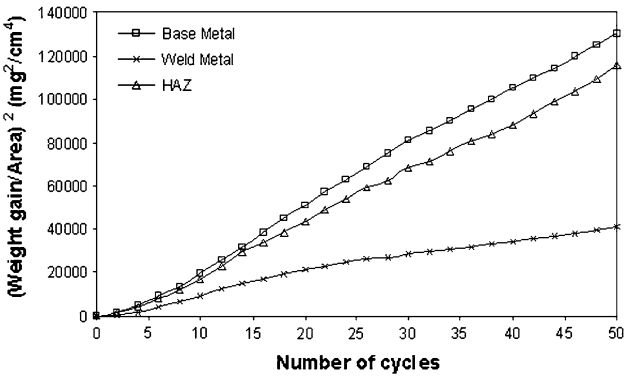

Fig. 3 Weight gain square (mg^2/cm^4) plot for different regions of TIG weldment in T22 steel exposed to cyclic hot corrosion in Na_2SO_4-60% V_2O_5 at 900 °C for 50 cycles

It can be inferred from Fig. 2 that the weight gain for base metal is much larger as compared to weld metal. The total weight gain after 50 cycles for base metal is around 1.78 times that of weld metal. All the regions of TIG weldment followed the parabolic behavior as can be inferred from the square of weight change (mg^2/cm^4) plotted with number of cycles in Fig. 3. The parabolic rate constants values are shown in Table 2.

3.3 Measurements of Oxide Scale Thicknesses

The thickness of the oxide scale formed on the base metal, weld metal, and HAZ was measured from the BSEI, along the cross section of the mounted samples. Images for all the samples are shown in Fig. 4. The thicknesses of the different regions of TIG weldment, as measured from the BSE images, are shown in Table 2.

3.4 X-ray Diffraction Analysis

The XRD patterns of the high temperature corroded specimens after 50 cycles have been shown in Fig. 5. These diffractograms reveal almost similar phases for all the steels. As obvious from the composition all the steels exhibited the formation of iron oxide (Fe_2O_3) as main phase along with weak peaks of Cr_2O_3. The XRD patterns for the oxidized sections of the base metal are different in intensity peak as compared to weld metal and the HAZ.

3.5 SEM/EDAX Analysis

The surface SEM/EDAX morphology of different regions of TIG weldment in 2.25Cr-1Mo boiler steel is shown in Fig. 6. EDAX analysis indicates that the top scale of weld metal consists of mainly Fe_2O_3 (96.57%) with MnO (2.85%) whereas inner scale contain SiO_2 (3.17%), Cr_2O_3 (1.24%), and MnO (1.88%) along with main phase Fe_2O_3 (92.83%). The SEM micrographs of HAZ region show more corrosion of grain boundary (Fig. 6b). The upper oxide scale mainly consists of MnO (4.59%) and Fe_2O_3 (94.64%). The inner scale along the boundary contains small amounts of SiO_2 (9.87%) and MnO (3.80%) with iron oxide Fe_2O_3 (85.63%) (point 1, Fig. 6b).

3.6 EPMA Analysis

The cross-sectional EPMA analysis of oxide scale of weld metal of TIG weldment in 2.25Cr-1Mo steel shown in Fig. 7 indicates mainly the presence of iron in the whole oxide scale. EPMA analysis of weld metal revealed chromium as a layer in the lower part of scale. Vanadium is also distributed in small concentration in the bottom scale. At some places small

Table 2 Average scale thickness (mm) and parabolic rate constants (K_p)

Materials	Scale thickness, mm	K_p, 10^{-8} g^2 cm^4 s^{-1}
Base metal	...	76.233
Weld metal	1.3	23.098
HAZ	1.170	65.408

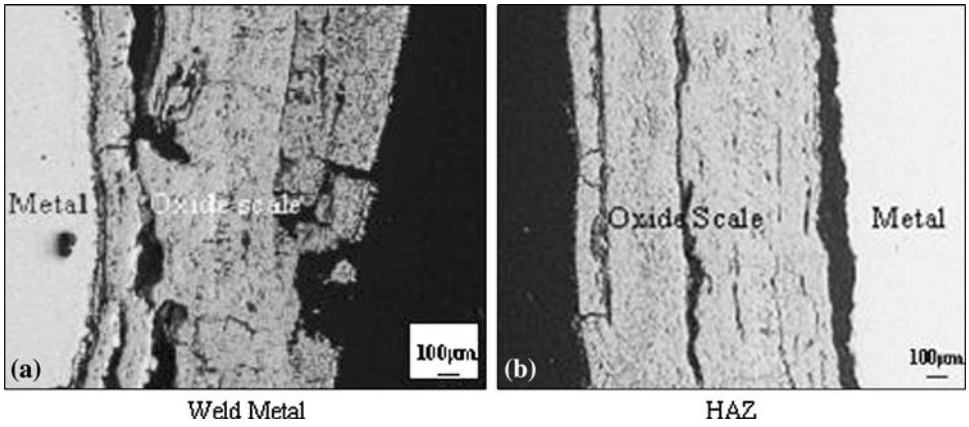

Fig. 4 B SEI micrographs showing cross section oxide scale morphology of different regions of TIG weldment (a) weld metal and (b) HAZ

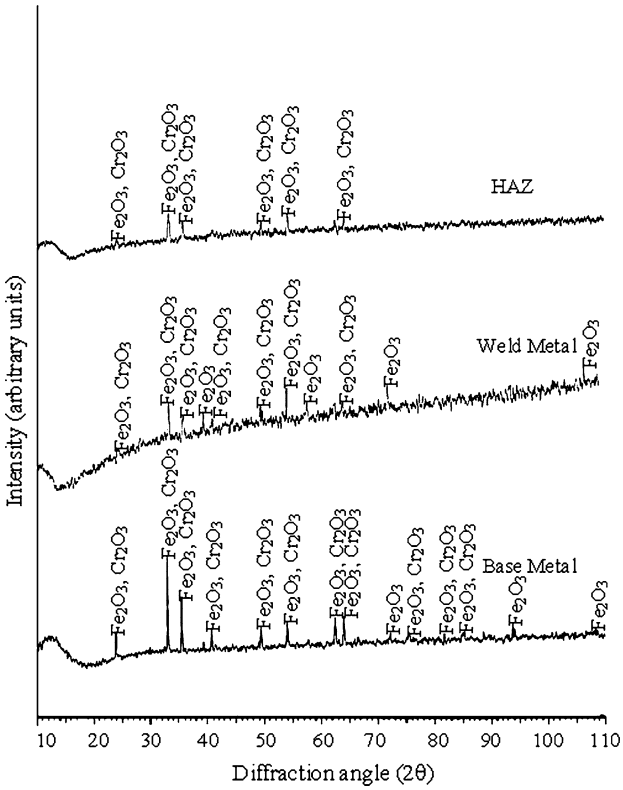

Fig. 5 X-ray diffraction profiles for different regions of TIG weldment in T22 steel exposed to cyclic hot corrosion in Na_2SO_4-60% V_2O_5 at 900 °C for 50 cycles

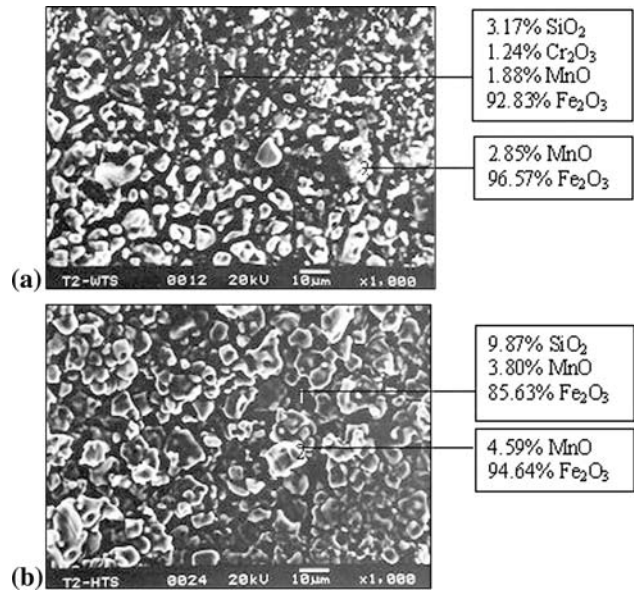

Fig. 6 Surface morphology and EDAX analysis for different regions of TIG weldment in T22 steel exposed to cyclic hot corrosion in Na_2SO_4-60% V_2O_5 at 900 °C for 50 cycles (a) weld metal, 1000× and (b) HAZ, 1000×

concentration of Na is also indicated in the upper and lower parts of the scale. EPMA shows (Fig. 8) that for HAZ where iron is the main element present throughout the scale sodium and vanadium are distributed in the whole scale equally. A small concentration of Cr is also indicated in the upper scale. Manganese is present in the upper layer of oxide scale.

The base metal showed intense spalling, peeling of scale, and enormous weight gain. The higher corrosion rate during initial hours of study, which might be attributed to the rapid oxygen pick up by diffusion of oxygen through the molten salt layer, is identical to the results reported by Sidhu and Prakash (Ref 9), Tiwari and Prakash (Ref 10), and Kumar et al. (Ref 7). The identification of Fe_2O_3 in the scales of base metal after hot corrosion experiments indicated that nonprotective conditions were established when Na_2SO_4-60% V_2O_5 molten salt was present on the surface. The formation of mainly Fe_2O_3 in the upper scale has also been reported to be nonprotective by Raman and Muddle (Ref 11). The base metal showed more weight gain than HAZ and weld metal and the reason may be the intense spalling and cracking of the oxide scale. The BSE image of the corroded HAZ shows that the scale has detached from the metal and cracked. From the scale thickness measurement (BSEI), it can be concluded that the multilayer scale on the HAZ specimen was thicker as compared to scale on the weld metal. Generally, thicker scales are more prone to spallation. It is important to note that even though the weld

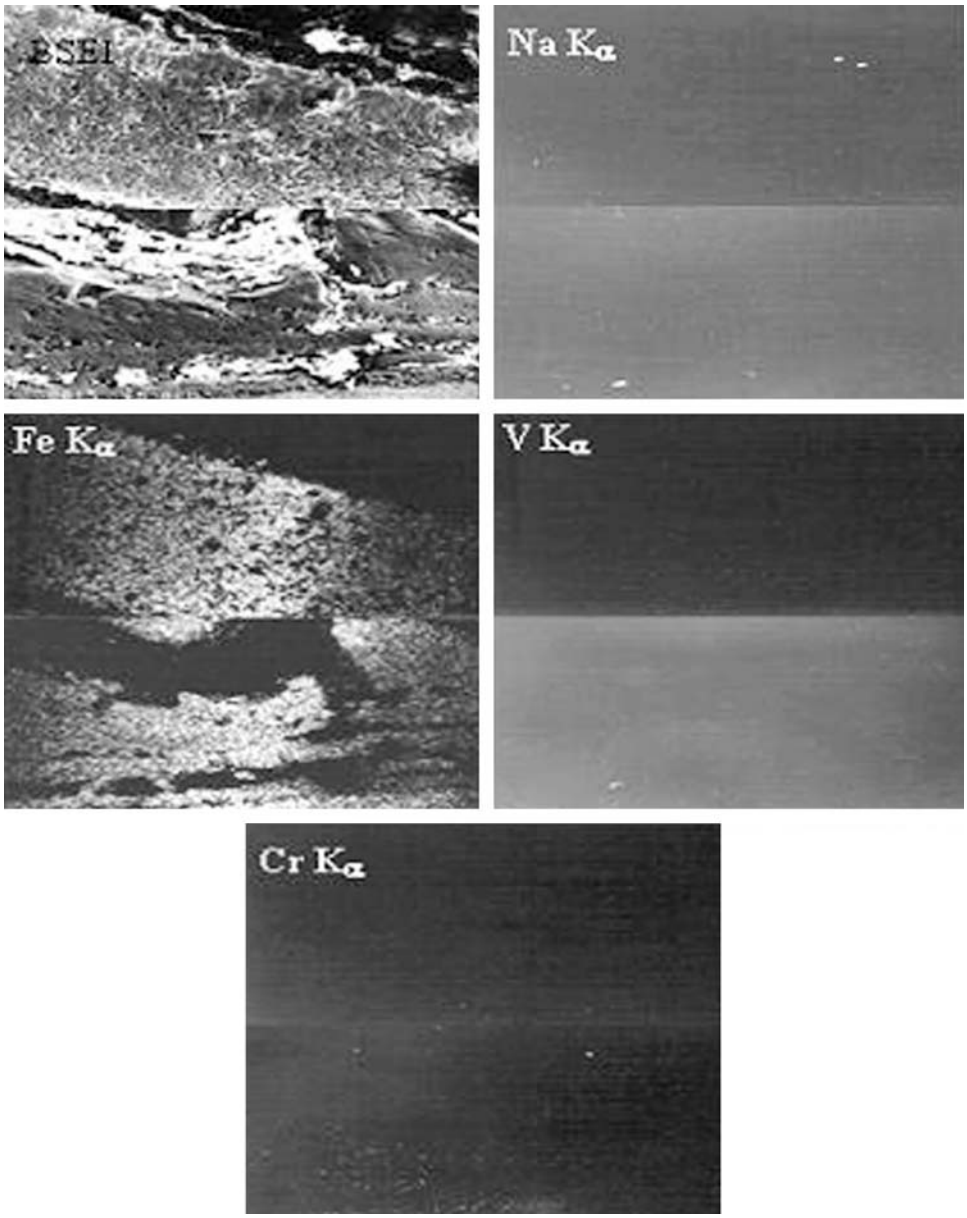

Fig. 7 B SEI and X-ray mapping of the cross section of weld metal of TIG weldment in T22 steel subjected to cyclic oxidation in Na_2SO_4-60% V_2O_5 at 900 °C for 50 cycles, 200×

metal oxidized at lower rates and formed a scale of lower thickness than the HAZ, it is the former that indicated a tendency for spallation after 17th cycle that became more prone to corrosion.

Further, it is confirmed by EPMA that the scale mainly contained oxide of iron with small concentration of chromium as shown in case of the scale on weld metal (Fig. 7). The higher weight gain of the HAZ and the formation of a thicker scale as compared to weld metal have been attributed to the absence of a protective inner scale of Fe-Cr oxides, due to the nonavailability of free Cr in this region (Fig. 8) as also discussed by Raman and Gnanamoorthy (Ref 12). The debonding at the metal/oxide interface for HAZ specimen might be contributed by formation and evaporation of MoO_3. This might have led to the acidic fluxing of the protective oxide scale. Identical results have been reported by Peters et al. (Ref 13), Fryburg et al. (Ref 14), and Pettit and Meier (Ref 15).

4. Conclusions

From the present studies, the following points are concluded.

1 The weld metal shows a combination of widmanstatten type ferrite, pearlite, and bainite. HAZ region showed coarse grain bainite.
2 When the base metal, weld metal, and the HAZ are oxidized in the molten salt environment; all of them follow parabolic kinetics. The weight gain of the base metal and HAZ were greater than that of weld metal. Even weld metal shows a little tendency for spallation and cracks during hot corrosion test. Fe_2O_3 was identified as the major phase by XRD, EDAX, and EPMA analysis in the scale of base metal, weld metal, and HAZ.

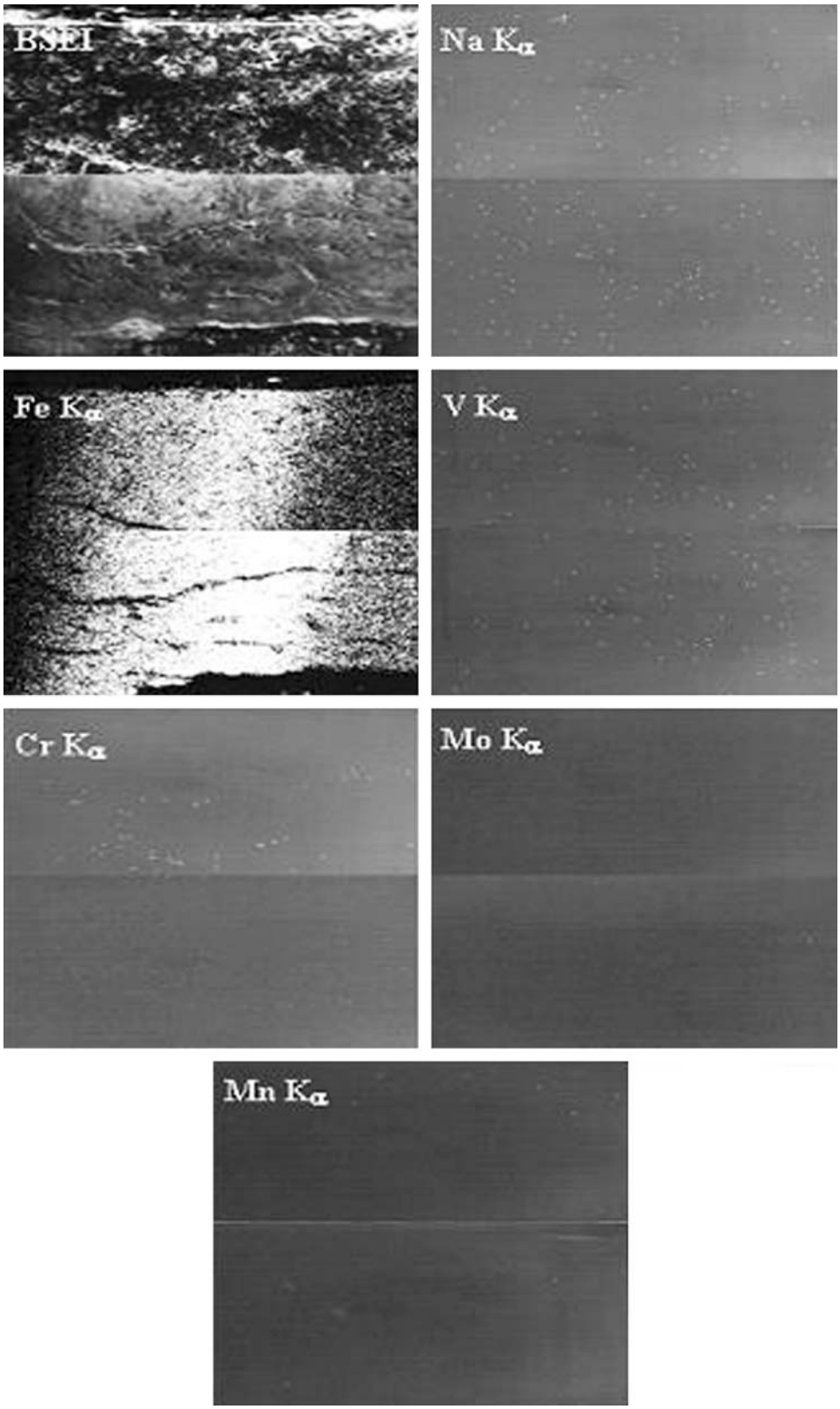

Fig. 8 B SEI and X-ray mapping of the cross section of HAZ of TIG weldment in T22 steel subjected to cyclic oxidation in Na_2SO_4-60% V_2O_5 at 900 °C for 50 cycles, 200×

3 The thicker oxide scale over HAZ was due to the formation of inner scales with free Cr than that of weld metal.

4 The corrosion rate (in terms of weight gain) of base metal, weld metal, and HAZ regions has been found in the following order base metal > HAZ > weld metal.

References

1. A. Al-Mazrouee, R.K.S. Raman, and R.N. Ibrahim, Effect of Post Weld Heat Treatment on the Oxide Scaling of Cr-Mo Steel Weldments, *J. Mater. Proc. Tech.*, 2005, **164–165**, p 964–970
2. R.K.S. Raman, A.S. Khanna, B.K. Choudhary, and J.B. Gnanamoorthy, Effect of Thermal Ageing on the Oxidation Behaviour of 9Cr-1Mo Steel, *Mater. Sci. Eng. A*, 1991, **148**, p 299–306
3. R.A. Rapp and Y.S. Zhang, Hot Corrosion of Materials: Fundamental Studies, *JOM*, 1994, **46**(12), p 47–55
4. S. Srikanth, B. Ravikumar, S.K. Das, K. Gopalakrishna, K. Nandakumar, and P. Vijayan, Analysis of Failures in Boiler Tubes Due to Fireside Corrosion in a Waste Heat Recovery Boiler, *Eng. Fail. Anal.*, 2003, **10**, p 59–66
5. A.S. Khanna and S.K. Jha, Degradation of Materials Under Hot Corrosion Conditions, *Trans. Indian Inst. Met.*, 1998, **51**(5), p 279–290
6. Y.S. Hwang and R.A. Rapp, Thermochemistry and Solubilities of Oxides in Sodium Sulfate-Vanadate Solutions, *Corrosion*, 1989, **45**(11), p 933–937
7. R. Kumar, V.K. Tewari, and S. Prakash, Studies on Hot Corrosion of the 2.25Cr-1Mo Boiler Tube Steel and Its Weldments in the Molten Salt Na_2SO_4–60 pct V_2O_5 Environment, *Mett. Mater. Trans. A*, 2007, **38**(1), p 54–57
8. S. Natarajan and S.P.K. Babu, Corrosion and Its Inhibition in SA213–T22 TIG Weldments Used in Power Plants under Neutral and Alkaline Environments, *Mater. Sci. Eng. A*, 2006, **432**, p 47–51
9. B.S. Sidhu and S. Prakash, Evaluation of the Corrosion Behaviour of Plasma-Sprayed Ni3Al Coatings on Steel in Oxidation and Molten Salt Environments at 900 °C, *Surf. Coat. Technol.*, 2003, **166**, p 89–100
10. S.N. Tiwari and S. Prakash, Studies on the Hot Corrosion Behaviour of Some Superalloys in Na_2SO_4-60% V_2O_5, *Paper Presented at Symposium on Localized Corrosion and Environmental Cracking (SOLCEC)*, C-33, Kalpakkam, India, 1997
11. R.K.S. Raman and B.C. Muddle, Role of High Temperature Corrosion in Life Assessment and Microstructural Degradation of Cr-Mo Steel Weldments, *Int. J. Press. Vessel Piping*, 2000, **77**, p 117–123
12. R.K.S. Raman and J.B. Gnanamoorthy, The Oxidation Behaviour of the Weld Metal, Heat Affected Zone and Base Metal in the Weldments of 2.25Cr-1Mo Steel, *Corros. Sci.*, 1993, **34**(8), p 1275–1288
13. K.R. Peters, D.P. Whittle, and J. Stringer, Oxidation and Hot Corrosion of Nickel-Based Alloys Containing Molybdenum, *Corros. Sci.*, 1976, **16**(11), p 791–804
14. G.C. Fryburg, F.J. Kohl, C.A. Stearns, and W.L. Fielder, Chemical Reactions Involved in the Initiation of Hot Corrosion of B-1900 and NASA-TRW VIA, *J. Electrochem. Soc*, 1982, **129**(3), p 571–585
15. F.S. Pettit, G.H. Meier, M. Gell, C.S. Kartovich, R.H. Bricknel, W.B. Kent, and J.F. Radovich, eds., *Oxidation and Hot Corrosion of Superalloys*, The Metal Society AIME, Warrendale, PA, 1984, p 651–687